J|A|C|S
ARTICLES
Published on Web 01/04/2007

A Fractional Bond Order of 1/2 in Pd_2^{5+}−Formamidinate Species; The Value of Very High-Field EPR Spectra

John F. Berry,*[,†,‡,§] Eckhard Bill,[†] Eberhard Bothe,[†] F. Albert Cotton,*[,‡] Naresh S. Dalal,*[,⊥] Sergey A. Ibragimov,[‡] Narpinder Kaur,[⊥] Chun Y. Liu,[‡] Carlos A. Murillo,*[,‡] Saritha Nellutla,[⊥] J. Micah North,[⊥] and Dino Villagrán[‡]

Contribution from the Department of Chemistry and Laboratory of Molecular Structure and Bonding, P.O. Box 30012, Texas A&M University, College Station, Texas 77842-3012, Department of Chemistry and Biochemistry, and Center for Magnetic Resonance, National High Magnetic Field Laboratory, Florida State University, Tallahassee, Florida 32306-4390, Department of Chemistry, 1101 University Avenue, University of Wisconsin, Madison, Wisconsin 53706-1322, and the Max-Planck-Institut für Bioanorganische Chemie, Stifstrasse 34-36, D-45470 Mülheim an der Ruhr, Germany

Received October 12, 2006; E-mail: murillo@tamu.edu

Abstract: Reaction of $Pd_2(DAniF)_4$, **1**, (DAniF = di-*p*-anisylformamidinate) with 1 equiv of $AgPF_6$ in CH_2Cl_2 at or below −10 °C produces the paramagnetic species $[Pd_2(DAniF)_4]PF_6$, **1-PF$_6$**, that has been studied by X-ray crystallography, UV−vis spectroscopy, electrochemistry, and multifrequency (9.5, 34.5, 110, and 220 GHz) EPR spectroscopy. Upon oxidation of the precursor, the Pd−Pd distance decreases by 0.052 Å from 2.6486(8) to 2.597(1) Å. The EPR spectra show broad signals with line widths of about 1000 G. The spectra collected at high field show a large spread of *g* tensor components (∼0.03), but these are masked at lower frequencies (9.5 and 34.5 GHz). A reinvestigation using high-field EPR of the *p*-tolyl analogue, which is the only other structurally characterized Pd_2^{5+} species (Cotton, F. A.; Matusz, M.; Poli, R.; Feng, X. *J. Am. Chem. Soc.* **1988**, *110*, 1144), shows that this species, which had been reported to give an isotropic 9.5 GHz EPR spectrum, also gives anisotropic 110 and 220 GHz EPR spectra with a similarly large spread of *g* tensor components consistent with the unpaired electron residing in a metal-based MO. The results of these studies and calculations using density functional theory are consistent with the oxidation being metal-based, resulting in an uncommon Pd_2^{5+} species with a Pd−Pd bond order of 1/2.

Introduction

The most common oxidation states of palladium are 0, 2, and 4, and well-characterized compounds containing one or more palladium(III) species are rare.[1,2] Often compounds such as PdF_3, whose formula suggests the possibility of having Pd^{III} species, actually contain Pd^{II} and Pd^{IV}.[3] These compounds are diamagnetic because neither the d^8 electronic configuration in square-planar Pd^{II} species nor the low-spin d^6 configuration in octahedral Pd^{IV} compounds has unpaired electrons. Of the four known paddlewheel compounds with a Pd_2^{6+} core, one has the formula $Pd_2(hpp)_4Cl_2$[4] (hpp = the anion of the guanidine-type compound 1,3,4,6,7,8-hexahydro-2*H*-pyrimido[1,2*a*]pyrimidine) and three have the general formula Pd_2(*cis*-orthometalated phosphine)$_2$(carboxylate)$_2Cl_2$.[5] These compounds are diamagnetic because of the formation of a Pd−Pd single bond. Two species containing what have been described as Pd_2^{5+} units are $[Pd_2(DTolF)_4]PF_6$, **2-PF$_6$** (DTolF = di-*p*-tolylformamidinate), which has been structurally characterized,[6] and an oxidized species formed during electrochemical oxidation of $Pd_2(DPhBz)_4$ (DPhBz = *N*,*N*′-diphenylbenzamidinate).[7]

What would appear to be conflicting data have been reported for these compounds. For the Pd−formamidinate compound, the X-band (∼9.6 GHz) EPR spectrum at 77 K in CH_2Cl_2 solution consisted of a single broad isotropic signal ($g_{av} = 2.014$) which was interpreted as arising from ligand-centered oxidation.[6] This conclusion was in agreement with the fact that the Pd⋯Pd distance in the crystal structure did not change significantly upon oxidation of the Pd_2^{4+} precursor, but it disagreed with the results of scattered wave Xα calculations that placed the unpaired electron in a Pd-based orbital of δ^* symmetry.[6] However, for the benzamidinate complex, a sharp axial signal ($g_{||} = 1.98$, $g_{\perp} = 2.17$, obtained at X-band frequency at 123 K in frozen CH_2Cl_2) showed side bands consistent with Pd hyperfine interactions (^{105}Pd has $I = 5/2$ and is 22.3% abundant

[†] Max-Planck-Institut.
[‡] Texas A&M University.
[§] University of Wisconsin.
[⊥] Florida State University.

(1) Cotton, F. A.; Wilkinson, G.; Murillo, C. A.; Bochmann, M. *Advanced Inorganic Chemistry*, 6th ed.; Wiley & Sons: New York, 1999.
(2) See: Liu, F.; Chen, W.; Wang, D. *J. Chem. Soc., Dalton Trans*. **2006**, 3445 and references therein.
(3) Tressaud, A.; Winterberger, M.; Bartlett, N.; Hagenmuller, P. *C. R. Acad. Sci.* **1976**, *282*, 1069.
(4) Cotton, F. A.; Gu, J.; Murillo, C. A.; Timmons, D. J. *J. Am. Chem. Soc.* **1998**, *120*, 13280.
(5) Cotton, F. A.; Koshevoy, I. O.; Lahuerta, P.; Murillo, C. A.; Sanaú, M.; Ubeda, M. A.; Zhao, Q. *J. Am. Chem. Soc.* **2006**, *128*, 13674.
(6) Cotton, F. A.; Matusz, M.; Poli, R.; Feng, X. J. *J. Am. Chem. Soc.* **1988**, *110*, 1144.
(7) Yao, C.-L.; He, L.-P.; Korp, J. D.; Bear, J. L. *Inorg. Chem.* **1988**, *27*, 4383.

in nature), suggesting that the oxidation is metal-centered.[7] However, the lack of structural characterization for this Pd−benzamidinate species makes further comparison difficult.

It should be noted that palladium compounds have general importance as catalysts and in other applications,[8] and mixed valence compounds of the heavier congener Pt have also been widely studied because of their utility as catalysts[9] and in medicine.[10] The so-called platinum blues, with partial metal−metal bond character, have been of special interest.[11] Because of this and our interest in metal−metal bonded compounds, a synthetic project dedicated to the preparation of paddlewheel compounds having a Pd_2^{4+} core was initiated. This was followed by an electrochemical study to identify potential candidates that could undergo oxidation to Pd_2^{5+} species[12] that may provide a basis for reconciling the seemingly contrary experimental results found in the two reported Pd_2^{5+} species.[6,7]

Here we report the structure of $[Pd_2(DAniF)_4]PF_6$ (DAniF = di-*p*-anisylformamidinate), **1-PF$_6$**, which shows that the Pd−Pd distance decreases by ca. 0.05 Å upon oxidation of $Pd_2(DAniF)_4$. The X-band EPR spectrum is qualitatively similar to the one reported for $[Pd_2(DTolF)_4]PF_6$, for which an isotropic *g* value of 2.014 was obtained.[6] This spectrum does not allow unambiguous assignment of the unpaired electron to either a metal-based or a ligand-based MO. By using the recently developed multifrequency/high-field EPR spectroscopy, distinct $g_\perp$ and $g_{||}$ values and a large spread of *g* tensor components are evident in the spectra. These results are consistent with a metal-based oxidation and the existence of a fractional bond order of 1/2. A reexamination of the EPR spectrum of **2-PF$_6$** using high-field (∼110 and 220 GHz) EPR spectroscopy also supports this formulation for the $[Pd_2(DTolF)_4]^+$ cation.

Results and Discussion

Synthesis and Crystal Structure. Preparation of $[Pd_2(DAniF)_4]PF_6$, **1-PF$_6$**, was carried out straightforwardly by allowing a solution of $AgPF_6$ in CH_2Cl_2 to diffuse into a solution of $Pd_2(DAniF)_4$ (**1**), but care had to be taken to keep the mixture at low temperature (−10 °C). The solid can be kept for several days at −20 °C, but it slowly decomposes at room temperature, even in the absence of air, and more rapidly in the presence of moisture or in a solution exposed to air.

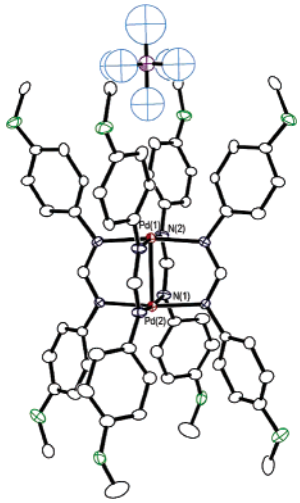

Figure 1. Structure of **1-PF$_6$** showing how the PF_6 anion rests above the pocket formed by the *p*-anisyl groups at a long distance from the Pd_2^{5+} unit. Displacement ellipsoids (anisotropic for the cation and isotropic for the anion) are drawn at the 30% probability level. Only one orientation for the disordered aryl groups and PF_6 anion is shown.

The structure of **1-PF$_6$** (Figure 1) shows a cation with a paddlewheel arrangement having an eclipsed configuration of the bridging ligands as does the precursor.[12] In this respect, it differs from the $Pd_2(DTolF)_4^+$ cation in **2-PF$_6$**, which has a N−Pd−Pd−N torsion angle of 17(1)°.[6] However, the most striking difference between these two compounds is the variation in the Pd−Pd distances. When $Pd_2(DTolF)_4$ is oxidized to $\mathbf{2}^+$, the metal−metal distance becomes 0.015 Å longer.[6] However, it is 0.052 Å shorter in the cation in **1-PF$_6$** than that in the precursor **1** (2.597(1) versus 2.6486(8) Å,[12] respectively). This shortening is about 50% of that observed when analogous Pt_2^{4+} compounds are oxidized to metal−metal bonded Pt_2^{5+} species.[13] A question that naturally arises is why there is such variation in the observed behavior of such metal−metal distances upon oxidation. To answer this question, one must consider that the bond order is only 1/2 and that there are two opposing forces that come into play when the dimetal units undergo oxidation: an increase in the positive charge is expected to increase electrostatic repulsions favoring an increase in the intermetal separation, while formation of a bond is expected to favor a decrease in the distance. A delicate balance of these forces is what determines the direction in which the Pd−Pd distance changes. An increase in electron-donating ability of the DAniF versus DTolF ligands would be expected to favor a decrease in the Pd···Pd distance because it would diminish the electrostatic repulsions between palladium atoms.[14] Very small variations in distances between metal atoms and changes that appear contrary to increases or decreases in bond order have also been observed in some Re_2^{n+} and $Tc_2^{5+/6+}$ complexes. For example, in the $[Re_2Cl_4(PMe_2Ph)_4]^{n+}$ species, $n = 0$, 1, and 2,[15] where the formal bond order decreases from 4 to 3.5 to 3, the Re−Re distances are 2.241(1), 2.218(1), and 2.215(2) Å, respectively.

(8) See, for example: (a) Leadbeater, N. E.; Marco, M. *J. Org. Chem.* **2003**, *68*, 888. (b) Zhao, F. Y.; Shirai, M.; Arai, M. *J. Mol. Catal. A: Chem.* **2000**, *154*, 39. (c) Bedford, R. B.; Blake, M. E.; Butts, C. P.; Holder, D. *Chem. Commun.* **2003**, 466. (d) Wolfe, J. P.; Singer, R. A.; Yang, B. H.; Buchwald, S. L. *J. Am. Chem. Soc.* **1999**, *121*, 9550. (e) Strieter, E. R.; Buchwald, S. L. Angew. *Chem., Int. Ed.* **2006**, *45*, 925. (f) Buchwald, S. L.; Mauger, C.; Mignani, G.; Scholz, U. *Adv. Synth. Catal.* **2006**, *348*, 23. (g) Tessier, D.; Rakai, A.; Bozon-Verduraz, F. *J. Chem. Soc., Faraday Trans.* **1992**, *88*, 741. (h) ten Brink, G.-T.; Arends, I. W. C. E.; Sheldon, R. A. *Science* **2000**, *287*, 1636. (i) Stahl, S. S. *Science* **2005**, *309*, 1824.
(9) See, for example: (a) Matsumoto, K.; Ochiai, M. *Coord. Chem. Rev.* **2002**, *231*, 229. (b) Matsumoto, K.; Sakai, K. *Adv. Inorg. Chem.* **2000**, *49*, 375. (c) Ochiai, M.; Lin, Y.-S.; Yamada, J.; Misawa, H.; Arai, S.; Matsumoto, K. *J. Am. Chem. Soc.* **2004**, *126*, 2536.
(10) See, for example: Lippert, B. *Coord. Chem. Rev.* **1999**, *182*, 263 and references therein.
(11) (a) Barton, J. K.; Rabinowitz, H. N.; Szalda, D. J.; Lippard, S. J. *J. Am. Chem. Soc.* **1977**, *99*, 2827. (b) Lippard, S. J. *Science* **1982**, *218*, 1075. (c) Ginsberg, A. P.; O'Halloran, T. V.; Fanwick, P. E.; Hollis, L. S.; Lippard, S. J. *J. Am. Chem. Soc.* **1984**, *106*, 5430. (d) Arrizabalaga, P.; Castan, P.; Geoffroy, M.; Laurent, J. P. *Inorg. Chem.* **1985**, *24*, 3656. (e) Lippert, B.; Schoellhorn, H.; Thewalt, U. *Inorg. Chem.* **1987**, *26*, 1736. (f) Sakai, K.; Matsumoto, K. *J. Am. Chem. Soc.* **1989**, *111*, 3074. (g) Sakai, K.; Matsumoto, K.; Nishio, K. *Chem. Lett.* **1991**, 1081. (h) Matsumoto, K.; Sakai, K.; Nishio, K.; Tokisue, Y.; Ito, R.; Nishide, T.; Shichi, Y. *J. Am. Chem. Soc.* **1992**, *114*, 8110. (i) Matsunami, J.; Urata, H.; Matsumoto, K. *Inorg. Chem.* **1995**, *34*, 202. (j) Mitewa, M. *Coord. Chem. Rev.* **1995**, *140*, 1.
(12) Berry, J. F.; Cotton, F. A.; Ibragimov, S. A.; Murillo, C. A.; Wang, X. *Inorg. Chem.* **2005**, *44*, 6129.
(13) Cotton, F. A.; Matonic, J. H.; Murillo, C. A. *Inorg. Chem.* **1996**, *35*, 498.
(14) A reviewer questioned whether the DAniF ligand or DArF ligands are flexible enough to allow the M−M bond to react to changes in bond order. In our experience, such ligands are so flexible that they can support metal−metal separations from about 2 Å to more than 3 Å. See, for example: Arnold, D. I.; Cotton, F. A.; Maloney, D. J.; Matonic, J. H.; Murillo, C. A. *Polyhedron* **1997**, *16*, 133 and references therein.

The last two distances are essentially the same within experimental error. In the quadruply bonded Tc_2^{6+} molecule $Tc_2(O_2CCH_3)_4Cl_2$,[16] the Tc−Tc bond distance of 2.192(1) Å is longer by 0.05 Å than that of 2.1260(5) Å in the Tc_2^{5+} anion $[Tc_2(O_2CCH_3)_4Cl_2]^-$, which has a formal bond order of 3.5.[17,18]

It should be noted that in crystals of **1-PF$_6$** the cation is *isolated*; axial ligands are absent. One of the fluoride atoms in the PF_6 anion is collinear with the M−M axis but the closest M···F distances of >5 Å are far too long to be chemically important. In this respect, it resembles $[Pd_2(DTolF)_4]PF_6$[6] and its Pt[13] and Ni[19] analogues. The absence of cation−anion bonding interactions in these compounds contrasts with the structures of many other mixed-valent "Pt_2^{5+}" complexes[20,21] such as those with bridging pyrophosphite ligands that tend to form Pt−Pt···X···Pt−Pt···X chains (X = halide) or the so-called charge density "wave" structures at low temperatures (i.e., $Pt^{2+}\cdots Pt^{2+}\cdots X-Pt^{3+}-Pt^{3+}-X\cdots$).[22]

EPR Spectroscopy. As mentioned in the Introduction, there have been two conflicting reports of Pd_2^{5+} paddlewheel species studied by EPR spectroscopy: one on the complex $[Pd_2(DTolF)_4]PF_6$ which has been characterized crystallographically,[6] and one on an oxidized species formed during coulometric oxidation of $Pd_2(DPhBz)_4$.[7] It should be noted that very few investigations of the EPR spectra of Pd^{III} species have been undertaken due to the rarity of isolable compounds having this ion. Some minerals and zeolites doped with Pd^{III} [23] as well as MCl-doped lattices (M = Na, K)[24] are known. There are several molecular compounds having tridentate macrocyclic ligands such as 1,4,7-triazacyclononane, *nido*-borane, or other ligands.[25−35] Most of the reported EPR spectra for these compounds have relatively broad bands with little anisotropy and g values close to the free electron value. With few exceptions, the reported g values range from 2.123 to 2.005, and in most cases $g_\perp$ is very close to $g_{||}$ and often larger than $g_{||}$ in agreement with axially elongated octahedral geometry.[36,37] The only Pd^{III} coordination compound in which the ^{105}Pd hyperfine structure is resolved in an EPR spectrum is $[Pd(1,4,7\text{-trithiacyclononane})_2]^{3+}$. For this species, which has been crystallographically characterized[33] and its EPR spectrum studied in frozen aqueous $HClO_4$ solution, A values of 20 and 5 G were reported.[38] In most other Pd^{III} species, the line width is typically between 100 and 200 G. Because of the broadness of such signals, splitting due to ^{105}Pd hyperfine interactions is not observed and generally hidden underneath the main signal.

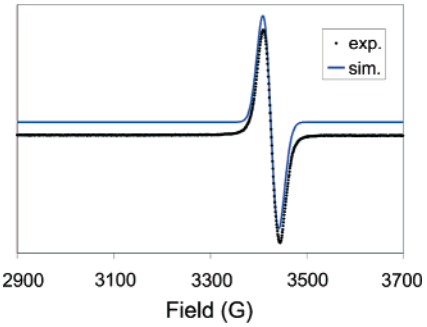

Figure 2. X-band EPR spectrum of coulometrically generated $[Pd_2(DAniF)_4]PF_6$, **1-PF$_6$**, taken in frozen CH_2Cl_2 at 25 K with a microwave frequency of 9.635426 GHz, power 200 μW, and modulation 3 mT. The simulation, shown above in blue, is based on spin Hamiltonian conventions with $S = 1/2$, with an isotropic g value of 2.01.

To investigate further the EPR properties of oxidized Pd_2−formamidinate complexes with the goal of unambiguously determining whether the unpaired electron is in a metal- or ligand-based MO, EPR spectra of $[Pd_2(DAniF)_4]PF_6$ were obtained under various conditions. First, an electrochemically generated solution of **1-PF$_6$** with a 1000-fold excess of NBu_4PF_6 in CH_2Cl_2 was frozen and an X-band EPR spectrum was obtained at 25 K; these conditions are comparable to those used in previous work with $[Pd_2(DTolF)_4]PF_6$.[6] This spectrum is shown in Figure 2, along with a simulation using an isotropic g value of 2.010. This spectrum is qualitatively and quantitatively similar to the one reported for **2-PF$_6$**, for which an isotropic g value of 2.014 was reported.[6] Under these conditions, determination of the type of MO being occupied by the unpaired electron is ambiguous. UV−vis data were also recorded during the coulometric oxidation, and the electronic spectrum of the oxidized species (Figure 3) agrees with the reported spectrum of **2-PF$_6$** as well as the spectrum from solutions made using **1-PF$_6$** crystals. Isosbestic points were observed in the monitored absorption spectra, indicating that the electrochemical process is reversible and that no decomposition of the species takes place on the time scale of the experiment.

When a 34.05 GHz (Q-band) spectrum of a powdered sample of $[Pd_2(DAniF)_4]PF_6$ was measured at near room temperature, the signal was exceptionally broad as shown in the upper part of Figure 4. As the temperature was lowered, the bandwidth decreased from 975 G at 295 K to 235 G at 10 K. These line widths are very broad and much wider than those commonly found in other Pd^{III} species (vide supra) or most other metal-

(15) See, for example: (a) Cotton, F. A.; Dunbar, K. R.; Falvello, L. R.; Tomás, M.; Walton, R. A. *J. Am. Chem. Soc.* **1983**, *105*, 4950 and references therein. (b) Bursten, B. E.; Cotton, F. A.; Fanwick, P. E.; Stanley, G. G.; Walton, R. A. *J. Am. Chem. Soc.* **1983**, *105*, 2606.
(16) Koz'min, P. A.; Larina, T. B.; Surazhskaya, M. D. *Sov. J. Coord. Chem.* **1982**, *8*, 451.
(17) Cotton, F. A.; Gage, L. D. *Nouv. J. Chim.* **1977**, *1*, 441.
(18) Sattelberger, A. P. In *Multiple Bonds between Metal Atoms*, 3rd ed.; Cotton, F. A., Murillo, C. A., Walton, R. A., Eds.; Springer Science and Business Media: New York, 2005; Chapter 7.
(19) Berry, J. F.; Bothe, E.; Cotton, F. A.; Ibragimov, S. A.; Murillo, C. A.; Villagrán, D.; Wang, X. *Inorg. Chem.* **2006**, *45*, 4396.
(20) Roundhill, D. M.; Gray, H. B.; Che, C.-M. *Acc. Chem. Res.* **1989**, *22*, 55.
(21) *Multiple Bonds between Metal Atoms*; Cotton, F. A., Murillo, C. A., Walton, R. A., Eds.; Springer Science and Business Media: New York, 2005.
(22) Yamashita, M.; Miya, S.; Kawashima, T.; Manabe, T.; Sonoyama, T.; Kitagawa, H.; Mitani, T.; Okamoto, H.; Ikeda, R. *J. Am. Chem. Soc.* **1999**, *121*, 2321.
(23) See, for example: Luca, V.; Kukkadapu, R.; Kevan, L. *J. Chem. Soc., Faraday Trans.* **1991**, *87*, 3083 and references therein.
(24) Vugman, N. V.; Netto Grillo, M. L.; Jain, V. K. *Chem. Phys. Lett.* **1992**, *188*, 419.
(25) Reid, G.; Blake, A. J.; Hyde, T. I.; Schröder, M. *J. Chem. Soc., Chem. Commun.* **1988**, 1397.
(26) McAuley, A.; Whitcombe, T. W. *Inorg. Chem.* **1988**, *27*, 3090.
(27) Jasper, S. A.; Huffman, J. C.; Todd, L. J. *Inorg. Chem.* **1998**, *37*, 6060.
(28) Chandrasekhar, S.; McAuley, A. *Inorg. Chem.* **1992**, *31*, 2663.
(29) Blake, A. J.; Crofts, R. D.; Degroot, B.; Schröder, M. *J. Chem. Soc., Dalton Trans.* **1993**, 485.
(30) Blake, A. J.; Reid, G.; Schröder, M. *J. Chem. Soc., Dalton Trans.* **1990**, 3363.
(31) Blake, A. J.; Gordon, L. M.; Holder, A. J.; Hyde, T. I.; Reid, G.; Schröder, M. *J. Chem. Soc., Chem. Commun.* **1988**, 1452.
(32) Blake, A. J.; Holder, A. J.; Hyde, T. I.; Roberts, Y. V.; Lavery, A. J.; Schröder, M. *J. Organomet. Chem.* **1987**, *323*, 261.
(33) Blake, A. J.; Holder, A. J.; Hyde, T. I.; Schröder, M. *J. Chem. Soc., Chem. Commun.* **1987**, 987.
(34) Blake, A. J.; Holder, A. J.; Hyde, T. I.; Schröder, M. *J. Chem. Soc., Chem. Commun.* **1987**, 1680.
(35) Möller, E.; Kirmse, R. *Inorg. Chim. Acta* **1997**, *257*, 273.
(36) A nice ligand field description of this is given by McAuley and Whitcombe. See ref 26.
(37) In Pd-containing species in montmorillonite (ref 23), the reported values of $g_{||}$ are larger than those for $g_\perp$.
(38) Fairly well-resolved spectra are also observed in palladium-doped montmorillonate. See ref 23.

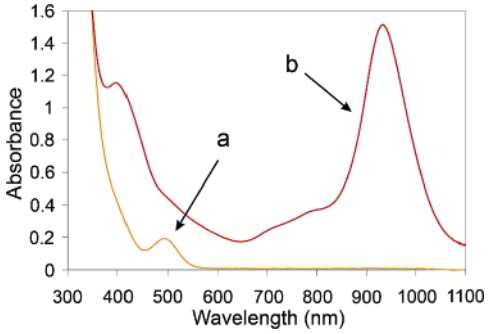

Figure 3. Electronic spectra of $Pd_2(DAniF)_4$ (a) and coulometrically prepared $[Pd_2(DAniF)_4]PF_6$ (b) recorded in CH_2Cl_2 solution at −25 °C with a concentration of 1.2 mM.

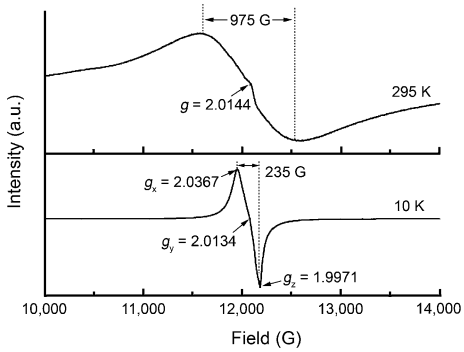

Figure 4. EPR spectra of **1-PF$_6$** at 34.05 GHz at 295 K (top) and 10 K (bottom). Note the large decrease in the line width at 10 K, ascribed to lifetime broadening of **1-PF$_6$**.

containing species. The large decrease in line width at low temperature probably originates from a short spin−lattice relaxation time that can only arise from a metal-containing paramagnetic species. The spectrum at 10 K implies that there are three g values ($g_x = 2.0367$, $g_y = 2.0134$, and $g_z = 1.9971$). Because this is consistent with rhombic symmetry (not tetragonal symmetry found in the crystal structure determined from data collected at 213 K), it is possible that a low-temperature phase transition takes place.[39]

The splitting of the g value into three g tensor components is more clearly established when the frequency is increased from 34.03 to 105.6 GHz (W-band) to 219.2 GHz (D-band EPR) as shown in Figure 5. At 4 K, the D-band EPR spectrum (lower section of Figure 5) shows values of $g_x = 2.0286$, $g_y = 2.0136$, and $g_z = 2.0004$.[40] Additional temperature dependence of the EPR spectra at 219.2 GHz is provided in Figure 6 and as Supporting Information (Figure S1). It should be noted that in some cases the W-band spectra of organic radicals may show well-separated g values. An example is that of a phenoxyl radical reported recently.[41] However, for such radicals the total spread of the g value components is still very small (2.0067 − 2.0022 = 0.0045) when compared with the spread in the EPR spectra for the Pd_2^{5+} species.[42] For example, for **1-PF$_6$** the spread in the X- and Q-band spectra of about ∼0.03 is about an order of

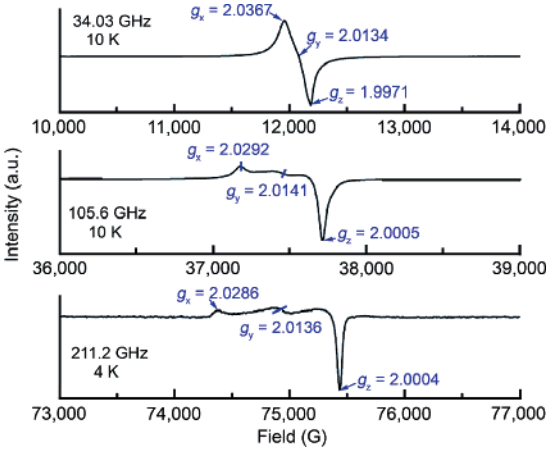

Figure 5. Comparison of EPR spectra of **1-PF$_6$** at 34.03, 105.6, and 211.2 GHz (as marked) at cryogenic temperatures. Note the splitting of the peak into three g tensor components, ranging from 2.0004 to 2.0290. The slightly smaller g values at 34 GHz relative to those at 105.6 and 211.2 GHz are ascribed to an incomplete peak resolution and to a lesser extent to residual order−disorder effects related to a postulated phase transition (see text).

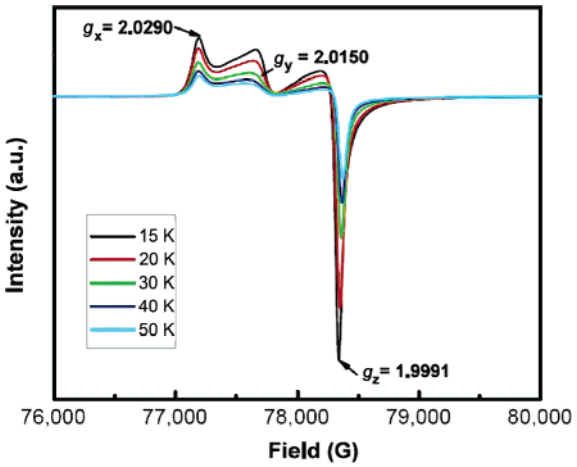

Figure 6. Temperature dependence of the EPR spectra of **1-PF$_6$** at 219.2 GHz in the low-temperature regime. The color code for the temperature is given in the inset.

magnitude larger than that for the free radical. This large spread in the g values can be ascribed to the large spin−orbit coupling of Pd, coupled to a lesser extent with some local fluxional behavior, as from an ensuing phase transition, as indicated by the lower-than-axial symmetry (three g components). Moreover, the line widths of the Pd_2−formamidinate compounds are about 2 orders of magnitude larger than those in the radical spectrum: 10 G for the radical versus >200 G for the Pd_2^{5+} system.[43] The excessive broadness of the band as well as the spread in g tensor components clearly support the assignment of the unpaired electrons of the Pd_2^{5+} species in the formamidinate compounds to mainly metal-based MOs. The broadness of the bands also suggests that there are MOs close in energy (vide infra).

It should be noted that further evidence showing that the unpaired electron is in a metal-based MO can be observed even

(39) It is not strictly necessary to invoke that a phase transition must occur because, as shown in the Experimental Section, one of the crystallographically independent ligands is disordered in the structure determined at 213 K. This might indicate that a less symmetric structure than what is implied by the tetragonal space group may exist. However, attempts to refine the structure in a less symmetric space group were unsatisfactory and provided higher refinement residuals.
(40) These g values are accurate to ±0.00005.
(41) Benisvy, L.; Bittl, R.; Bothe, E.; Garner, C. D.; McMaster, J.; Ross, S.; Teutloff, C.; Neese, F. *Angew. Chem., Int. Ed.* **2005**, *44*, 5314.
(42) For other examples on the use of high-field spectroscopy in systems of biological interest, see: (a) Kay, C. W.; Bittl, R.; Bacher, A.; Richter, G.; Weber, S. *J. Am. Chem. Soc.* **2005**, *127*, 10780. (b) Anderson, K. K.; Schmidt, P. P.; Katterle, B.; Stand, K. R.; Palmer, A. E.; Lee, S.-K.; Solomon, E. I.; Gräslund, A.; Barra, A.-L. *J. Biol. Inorg. Chem.* **2003**, *8*, 235. (c) Un, S.; Gerez, C.; Elleingand, E.; Fontecave, M. *J. Am. Chem. Soc.* **2001**, *123*, 3048.

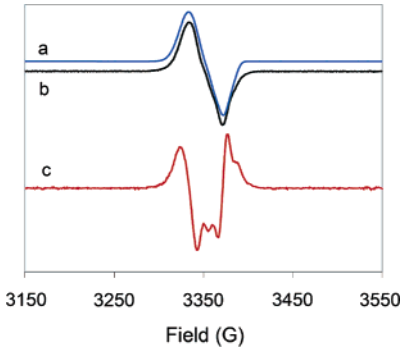

Figure 7. X-band EPR spectrum (b) of coulometrically generated $[Pd_2(DAniF)_4]PF_6$ recorded in frozen butyronitrile at 25 K with microwave frequency 9.431756 GHz, power 100 μW, and modulation 4 G. The simulation (a) is based on spin Hamiltonian conventions with $S = 1/2$, with axial g values of $g_\perp = 2.0212$, $g_{||} = 1.998$, and hyperfine interactions to two ^{14}N nuclei with $A_{||} = 5.7 \times 10^{-4}$ cm^{-1}.

when an X-band spectrum is measured in solution under special conditions. When the EPR spectrum at 25 K was recorded after a 0.10 mM $Pd_2(DAniF)_4$ solution was coulometrically oxidized in BuCN with 0.1 M $NBu_4[B(C_6F_5)_4]$ and then a frozen solution was prepared, this spectrum (Figure 7) is slightly but significantly changed from that in Figure 2 in which BuCN was not added. Notably, the negative peak of the derivative signal is sharper than the positive peak and has multiple inflection points indicative of hyperfine splitting. These inflections are more clearly recognized in the second derivative spectrum shown in Figure 7c where they appear clearly as peaks. Spectrum (b) could not be successfully simulated only by using an isotropic Lorentzian or Gaussian derivative line. This simulation yielded the following parameters: $g_\perp = 2.0212$, $g_{||} = 1.998$, $g_{iso} = (2g_\perp + g_{||})/3 = 2.013$. Because it is known that many dimetal units may add one or two axial ligands,[21] possible axial coordination by BuCN molecules was considered. Under these conditions, the simulation improved by addition of hyperfine interactions from two equivalent ^{14}N nuclei; a value of $A_{||} = 5.7 \times 10^{-4}$ cm^{-1} was used.[44] This causes the $g_{||}$ signal to be split into five signals which appear as added inflection points with an intensity ratio of 1:2:3:2:1; simulations assuming that eight equivalent ^{14}N nuclei (i.e., from the formamidinate ligands) are coupled to the $g_{||}$ signal led to simulated spectra with too many hyperfine lines. In addition, simulation of the second derivative spectrum using a model in which the unpaired electron is coupled to two ^{14}N nuclei gives reasonable agreement, albeit with a large uncertainty in the magnitude of the coupling (see Figure S2).

In view of the EPR results from **1-PF$_6$**, we decided to reinvestigate the previously reported $[Pd_2(DTolF)_4]PF_6$ compound.[6] When the 208 GHz (D-band) EPR spectrum of a powder of **2-PF$_6$** was measured at various temperatures ranging from near room temperature to 5 K, behavior similar to that of the DAniF analogue was observed. As shown in Figure 8, at 285 K there is a broad band (line width of 1295 G). Below about 200 K, the spectral width becomes much narrower, again likely

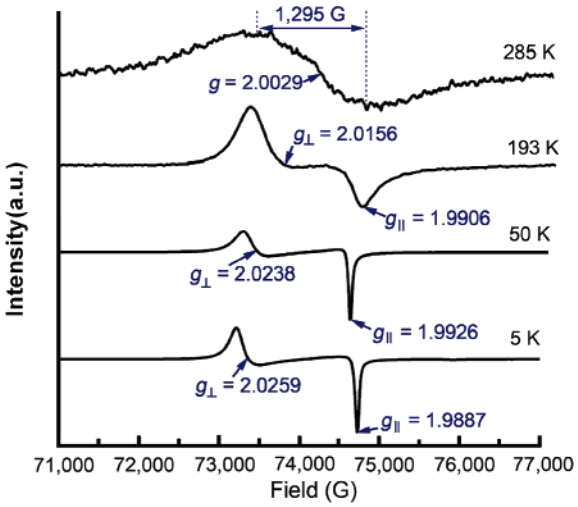

Figure 8. Temperature dependence of the EPR spectra of $[Pd_2(DTolF)_4]PF_6$ at 208 GHz, at temperatures of 285, 193, 50, and 5 K. Notice that the tetragonal symmetry persists from room temperature down to 5 K, which is consistent with an absence of a phase transition in this compound, in contrast to **1-PF$_6$** (see text).

due to the slowing down of some motional-averaging process. Axial symmetry is clearly visible at 193 K as manifested by the splitting of the g tensor components into two values. Because there is no phase transition observed upon lowering the temperature, the tetragonal symmetry in **2-PF$_6$** must persist through the temperature range of the study. At 5 K, these values are $g_\perp = 2.0259$ and $g_{||} = 1.9887$.[45] Additional EPR spectra showing the temperature dependence at 208 GHz are provided as Figure S3 in the Supporting Information. Again, a large spread of g value components ($\sim$0.03) implies a metal-based oxidation involving a single electron. The broadness of the band as well as the spread in the g tensor components again indicate that the unpaired electron is in a metal-based MO. Furthermore, the persistence of axial symmetry down to 5 K in $[Pd_2(DTolF)_4]PF_6$ indicates that the broadness in the spectra of **1-PF$_6$** cannot be attributed solely to the rotational disorder of the $-OCH_3$ moieties.

Some qualitative arguments based on a simple crystal-field model can be used to explain the possible origin of the large-tensor anisotropy as well as the broadness of the EPR signals. The g tensor components for a transition ion are directly related to the spin–orbit coupling constant via[46,47]

$$g_{||} - g_\perp = 2\lambda/[(1/E1) - (4/E2)]$$

where λ is the spin–orbit coupling for the transition ion, and E1 and E2 are the energy difference between the ground-state orbital and the appropriate excited-state orbital that mixes with the ground state in the presence of the spin–orbit interaction. The use of this relationship has worked well for a Cr_2^{5+}–guanidinate species[45] and other Cr^{5+} compounds.[48] Considering that

(43) It should be noted that the high-field EPR spectra of the solid samples do not reflect randomly oriented crystallites in the solids, but show that there are preferred orientations of the crystallites. This explains why in the W- and D-band spectra shown here the g_z signals are much more intense than the g_x and g_y signals.

(44) Note that, even though the spherical PF_6 anions in **1-PF$_6$** do not interact with the Pd_2^{5+} unit in the solid state (Figure 1), the BuCN molecules are slimmer and more likely to interact with the dimetal unit than the hexafluorophosphate anions.

(45) For this compound, $g_\perp > g_{||}$. This is similar to what was found in a rare compound containing a Cr_2^{5+} core in which the unpaired electron is in a metal-based MO. See: Cotton, F. A.; Dalal, N. S.; Hillard, E. A.; Huang, P.; Murillo, C. A.; Ramsey, C. M. *Inorg. Chem.* **2003**, *42*, 1388.

(46) Weil, J. A.; Bolton, J. R.; Wertz, J. E. *Electron Paramagnetic Resonance*; Wiley & Sons: New York, 1994; p 223.

(47) (a) McGarvey, B. R. In *Electron Spin Resonance of Metal Complexes*; Yen, T. F., Ed.; Plenum: New York, 1969; Chapter 8. (b) McGarvey, B. R. *J. Phys. Chem.* **1967**, *71*, 51.

(48) Dalal, N. S.; Millar, J. M.; Jagadeesh, M. S.; Seehra, M .S. *J. Chem. Phys.* **1981**, *74*, 1916.

Scheme 1

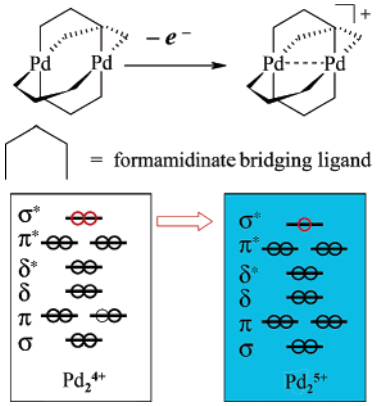

the spin−orbit coupling constant for the Cr ion is about 500 cm^{-1}, while that for the Pd ions is about 1600 cm^{-1},[46] the expected spread of the *g* components for the Pd system should be at least 6 times larger than that for a Cr analogue, if there is no large difference in energy between the orbitals for the two metal species. Because the *g* value spread for the Cr_2^{5+} species was 0.0066, a prediction of the *g* spread for the Pd_2^{5+} ion would be ~0.03 to 0.04, which is roughly the measured value of ~0.03. Such a spread in the *g* values would suggest a corresponding EPR signal line width of about 1000 G at 220 GHz, as found for the ambient temperature spectra for the Pd_2^{5+} species. Admittedly, this is only a rough approximation to explain the magnitudes of the *g* tensor components, especially since $g_{||}$ is lower than 2.0023, while $g_{\perp}$ is much larger than 2.0023.

Electronic Structure. In previous work on Pd_2 complexes,[6] SCF−Xα−SW calculations of the electronic structures of the Pd_2^{4+} and Pd_2^{5+} complexes were done using a model in which the aryl groups of the formamidinate ligands were replaced by H atoms. These results showed that many of the orbitals of the idealized M−M bonding manifold (i.e., Scheme 1) are perturbed in energy due to interactions with ligand-based orbitals and that there is significant mixing of the metal and ligand π orbitals. It is interesting to note that calculations of the electronic structure of the analogous dimolybdenum model, $Mo_2(HNCHNH)_4$, showed very little deviation from the orbital ordering given in Scheme 1 and also very little mixing of the Mo d orbitals with the ligand π orbitals.[49] This difference between the Pd_2 model and the Mo_2 model can be attributed to the increased effective nuclear charge of the Pd atom as compared to that of Mo, which causes the d orbitals of the former to contract and have lower energy (due to the increased stabilizing electron−nuclear interactions), and thus the Pd-based orbitals can be considered to be quite close in energy to the energies of the ligand π orbitals.

The previous Xα calculations[6] showed many of the orbitals of interest (HOMO, HOMO−1, HOMO−2, etc.) to be quite close in energy (<0.1 eV in several cases), and they also showed that the ordering is sensitive to subtle effects such as lowered symmetry from D_{4h} to D_4.[6] Moreover, the SOMO calculated for $[Pd_2(HNCHNH)_4]^+$ was a δ* orbital with significant ligand character that is formed from the two d_{xy} orbitals of the metal atoms and the π orbitals of the formamidinate ligands.[6] This was interpreted as not being in accord with the experimental data because $[Pd_2(DTolF)_4]^+$ was believed to contain a ligand-centered radical.[6]

(49) Cotton, F. A.; Feng, X.; Matusz, M. *Inorg. Chem.* **1989**, *28*, 594.

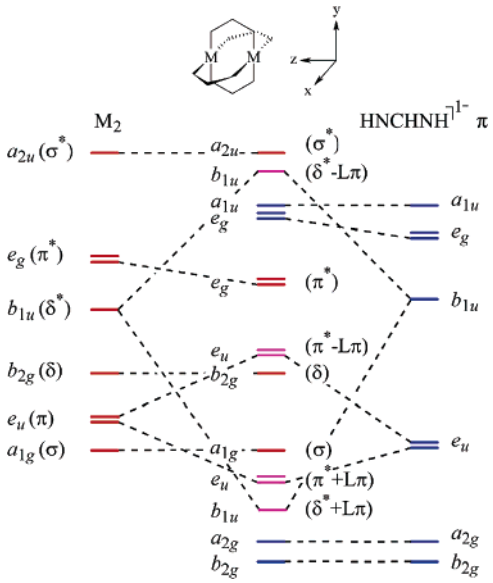

Figure 9. Schematic molecular orbital diagram showing the interactions of the HNCHNH π orbitals with the metal−metal bonding manifold. The red orbitals are purely metal-based, the blue orbitals are purely ligand-based, and the purple orbitals are highly mixed metal−ligand orbitals.

Scheme 2

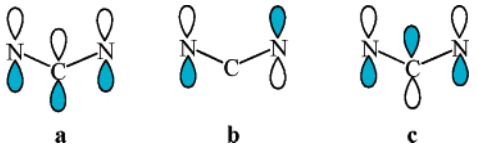

We have reexamined the problem of the electronic structures of $Pd_2^{4+/5+}$ complexes using current levels of theory. For this investigation, we employed the B3LYP functional which has been used successfully in our laboratory[50] and elsewhere[51] for analysis of the electronic structures of metal−metal bonded systems. In this case, we optimized the geometry of the model by starting from the atomic coordinates of the crystal structure of $Pd_2(DTolF)_4$, which presents a twisted (17°) conformation of D_4 symmetry. For completeness, two different calculations were performed with two different basis sets of double- and triple-ζ quality, as described in the Experimental Section on computational details. The calculated optimized geometry of the dipalladium model results in an untwisted conformation, D_{4h} symmetry, regardless of either the starting geometry or the basis set. The Pd−Pd distance, nominally with a bond order of zero, was calculated to be 2.739 and 2.731 Å with the double- and triple-ζ basis sets, respectively.

The results of these calculations can be explained in terms of a perturbation of the idealized M−M manifold (Scheme 1) by interactions with the π orbitals of the HNCHNH units (shown diagrammatically in Scheme 2 and Figure 9). Similarly to the Ni_2^{5+} compounds described earlier,[19] each formamidinate ligand has a bonding (a), nonbonding (b), and antibonding (c)

(50) (a) Cotton, F. A.; Donahue, J. P.; Murillo, C. A.; Pérez, L. M. *J. Am. Chem. Soc.* **2003**, *125*, 5486. (b) Cotton, F. A.; Donahue, J. P.; Hall, M. B.; Murillo, C. A.; Villagrán, D. *Inorg. Chem.* **2004**, *43*, 6954. (c) Cotton, F. A.; Liu, C. Y.; Murillo, C. A.; Villagrán, D.; Wang, X. *J. Am. Chem. Soc.* **2003**, *125*, 13564.

(51) See, for example: (a) Chisholm, M. H.; Click, D. R.; Galluci, J. C.; Hadad, C. M.; Wilson, P. J. *Organometallics* **2003**, *22*, 4725. (b) Chisholm, M. H.; Davidson, E. R.; Quinlan, K. B. *J. Am. Chem. Soc.* **2002**, *124*, 15351. (c) Lichtenberger, D. L.; Lynn, M. A.; Chisholm, M. H. *J. Am. Chem. Soc.* **1999**, *121*, 12167.

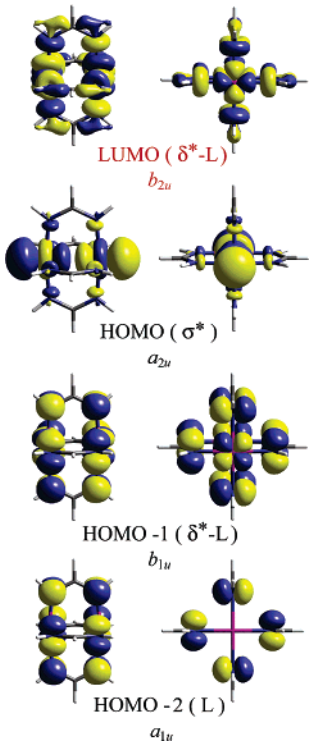

Figure 10. Surface contour diagrams from DFT (0.04 isodensity) of the three highest occupied and the lowest unoccupied molecular orbitals for the $Pd_2(HNCHNH)_4$ model.

combination of π orbitals (Scheme 2). These combine to form 12 molecular orbitals for the $M_2(HNCHNH)_4$ species in D_{4h} symmetry, disposed as shown in the right-hand column of Figure 9.[52] Shown in the left-hand column of this figure are the orbitals of the idealized M−M bonding manifold.[53]

Symmetry-matched interactions between the M_2 orbitals and the formamidinate π orbitals result in the central column of Figure 9. Orbitals for which there is no symmetry match (M_2 σ a_{1g}, L π a_{2g}, L π a_{1u}, and M_2 σ^* a_{2u}) are drawn in the central column unchanged in energy from their original positions. Several of the orbitals that could interact (the e_g set and the b_{2g} set) are calculated to be only slightly perturbed from their original energies, although the b_{1u} and e_u sets of orbitals are highly perturbed. The most important of these interactions occurs with the b_{1u} orbitals, which overlap so strongly that their antibonding combination ($\delta^*-L\pi$) is very near in energy to the HOMO (σ^*). Figure 10 shows contour plots of the frontier molecular orbitals of the $Pd_2(HNCHNH)_4$ model. It should be noted here that the LUMO is an orbital of δ^* symmetry formed by the $d_{x^2-y^2}$ orbitals and which has significant antibonding interactions with the σ orbitals of the HNCHNH ligands.

Also shown in Figure 9 are qualitative estimates of the metal/ligand contributions to the molecular orbitals. Orbitals shown in red are essentially pure metal orbitals with little or no contributions from the ligands. Orbitals in blue are essentially ligand-based orbitals having very little metal character. The orbitals in purple are *highly mixed* and having nearly equal metal and ligand contributions. It should be noted that, upon improving the basis set from double-ζ to triple-ζ, the energies of the frontier orbitals are better resolved. With the orbital diagram (Figure 9) available, we can now begin to understand many of the puzzling properties of the compounds. To begin, it is clear why four reversible oxidations can be observed electrochemically in the CV of **1** (Figure 11).[54] The reason is that the HOMO and HOMO−1 are very close in energy (with the double-ζ basis set those values were essentially the same; improving the basis set to triple-ζ resolved the difference by 0.2 eV), and thus the four electrons that occupy these two orbitals are easily removed at very similar electrochemical potentials. Also, the absorption spectrum of the Pd_2^{5+} species has a very intense band at rather low energy (ca. 900 nm), which may be due to a HOMO−1 → SOMO transition that would have some characteristics of an LMCT transition. Second, based on the MO diagram in Figure 9, Koopmanns' theorem predicts that one-electron oxidation involves removal of an electron from metal-based orbitals producing true Pd_2^{5+} units rather than ligand-centered radicals. Moreover, density functional theory (DFT) calculations of the singly oxidized species $M_2(HNCHNH)_4^+$, performed using an open-shell geometry optimization to a singly oxidized model using the double-ζ basis set, also show clearly that the SOMO in each case is the metal-based a_{2u} σ^* orbital. The calculated contraction of the Pd−Pd distance by about 0.026 Å is consistent with the experimental value (0.052 Å) and the formulation of its electronic structure, namely the formation of a bond order of 1/2. Furthermore, the metal-based MOs are close in energy and considerable mixing is expected. This mixing is an important factor that contributes to the broadness of the EPR signals.

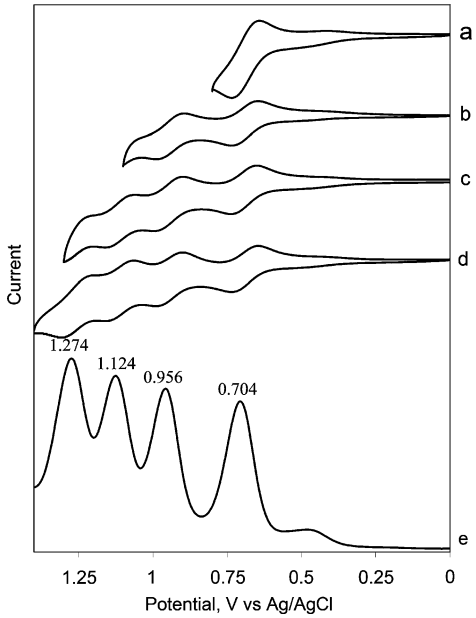

Figure 11. CVs (a−d) and DPV (e) of $Pd_2(DAniF)_4$ measured in CH_2Cl_2 solution showing the four closely spaced oxidation processes that occur between 0.704 and 1.274 V vs Ag/AgCl.

Finally, it should be noted that even though results from Xα calculations and those from DFT calculations give different symmetry labels for the HOMO (δ^* for Xα and σ^* for DFT calculations), the results in both types of calculations are consistent in that the MOs are close in energy.

(52) Only the first eight of these orbitals are shown, since the other four (a_{2g}^*, e_u^*, and b_{2g}^*) are vacant and strongly antibonding and thus too high in energy to be of importance to this discussion.

(53) The set of δ and δ^* orbitals arising from the overlap of the $d_{x^2-y^2}$ functions is not shown as these orbitals are vacant and high in energy and thus not relevant to our discussion.

(54) Four oxidation processes were also observed for the analogous $[Ni_2(DAniF)_4]PF_6$ compound. See ref 12.

Conclusions

On the basis of a combination of techniques such as X-ray crystallography, electrochemistry, electronic structure calculations, and the recently developed multifrequency/high-field EPR spectroscopy over a wide temperature range down to 4 K, we have resolved a long-standing controversy on the electronic structure of the Pd_2^{5+}−formamidinate paddlewheel compounds and shown conclusively that the unpaired electron is located in a mainly metal-based molecular orbital. The one-electron metal−metal bond is formed in a manner similar to that in the other group 10 M_2^{5+}−formamidinates, M = Ni[19] and Pt.[13] Depending on the electron-donating abilities of the bridging ligand, which compensates for increased electrostatic repulsion between two Pd centers, the response of the metal−metal distance to the electron loss is variable. In the case of DAniF, it significantly decreases, whereas in the case of DTolF, where the ligand is less basic, there is a slight increase.

It should be emphasized that the conclusions of this study would not have been unequivocal without the results from such a variety of techniques, and our newfound understanding of the electronic structure of these Pd_2^{5+} species is the result of modern advances in theory and EPR experimentation. The utility of variable-temperature, high-field EPR spectroscopy in determining unambiguously the location of the unpaired electrons in dimetal species (e.g., those with Pd_2^{5+} units) has been clearly established. These techniques will undoubtedly be of importance in other systems resolving questions regarding MOs containing unpaired electrons.

Experimental Section

Materials and Methods. All manipulations were carried out under an atmosphere of dry nitrogen gas using standard Schlenk techniques. Solvents were either distilled over appropriate drying agents in a nitrogen atmosphere or purified using a Glass Contour solvent system. The Pd_2^{4+} precursors $Pd_2(DAniF)_4$[12] and $Pd_2(DTolF)_4$[6] were synthesized according to the published procedures. The oxidized $[Pd_2(DTolF)_4]PF_6$[6] salt was prepared similarly to **1-PF$_6$** (vide infra).

Physical Measurements. The IR spectra were collected on a Perkin-Elmer 16PC FTIR spectrometer using KBr pellets. Differential pulse voltammograms (DPVs) and cyclic voltammograms (CVs) were taken on a CH Instruments electrochemical analyzer using dichloromethane solutions with 1 M NBu_4PF_6 and 0.1 mM analyte. The electrodes were: Pt disk (working), Pt wire (auxiliary), and Ag/AgCl (reference). Under these conditions, the redox couple for ferrocene/ferrocenium consistently appeared at +450 mV. Elemental analyses were carried out by Canadian Microanalytical Services in British Columbia, Canada. Visible spectra were obtained on a Shimadzu UV-2501 PC UV−vis spectrophotometer. Spectroelectrochemistry was performed at −25 °C using an EG&G potentiostat/galvanostat with 0.1 M NBu_4PF_6 with a Pt net working electrode, a Pt net auxiliary electrode, and an $Ag/AgNO_3$ reference electrode. During coulometry, electronic spectra were monitored using an HP 8453 spectrophotometer (range: 190−1100 nm). EPR measurements were made using finely divided, powdered compounds at the 9.5 GHz (X-band), 34 GHz (Q-band), 105 GHz (W-band), and 210 GHz (D-band) microwave frequencies. The X- and Q-band spectra were collected using a Bruker EMX spectrometer, fitted with frequency counters, gauss meters, and Oxford helium flow cryostats for variable-temperature studies done in the range of 4−350 K. The W-band and D-band measurements were at the National High Magnetic Field Laboratory in Tallahassee, Florida, using a custom-built variable-frequency EPR spectrometer that has been described elsewhere.[55]

Table 1. Crystal Data for **1-PF$_6$**

formula	$C_{60}H_{60}F_6N_8O_8PPd_2$
fw	1378.93
cryst system	tetragonal
space group	*P*4/*n*
a (Å)	12.947(1)
b (Å)	12.947(1)
c (Å)	17.540(4)
V (Å^3)	2940.1(8)
Z	2
d_{calcd} (g cm^{-3})	1.558
R1,[a] wR2[b] ($I > 2\sigma(I)$)	0.0536, 0.1511
R1,[a] wR2[b] (all data)	0.0714, 0.1667

[a] $R1 = \sum||F_o| - |F_c||/\sum|F_o|$. [b] $wR2 = \{\sum[w(F_o^2 - F_c^2)^2]/\sum[w(F_o^2)^2]\}^{1/2}$, $w = 1/\sigma^2(F_o^2) + (aP)^2 + bP$, where $P = [\max(0 \text{ or } F_o^2) + 2(F_c^2)]/3$.

Synthesis of $[Pd_2(DAniF)_4]PF_6$, 1-PF$_6$. To a solution of $Pd_2(DAniF)_4$ (350 mg, 0.284 mmol) in 10 mL of CH_2Cl_2 was added $AgPF_6$ (72.0 mg, 0.284 mmol) dissolved in 10 mL of CH_2Cl_2 at −70 °C. An immediate color change from orange to black was observed. The mixture was stirred for 10 min at −70 °C, followed by filtration through Celite. A dark-green powder was precipitated by addition of ether and dried under vacuum. Yield: 0.275 g, 70%. X-ray quality crystals were obtained by dissolving **1** (20 mg, 0.016 mmol) in 4.0 mL of CH_2Cl_2 and then adding a layer of 2.0 mL of benzene on top of the solution. This mixture was held at −70 °C until the benzene layer froze. On top of the solid benzene was added a solution of $AgPF_6$ (7.0 mg, 0.030 mmol) in 10 mL of diethyl ether. This mixture was kept at −10 °C to allow the benzene to melt slowly by dissolving into the Et_2O. In 5 days, large black crystals of **1-PF$_6$** were isolated by filtration. Anal. Calcd for $C_{60}H_{62}N_8O_9Pd_2PF_6$: C, 51.59; H, 4.47; N, 8.02%. Found: C, 51.15; H, 4.34; N, 7.90%. IR (KBr, cm^{-1}): 1608 m, 1591 s, 1499 vs, 1464 w, 1438 w, 1423 w, 1325 vw, 1294 m, 1246 vs, 1226 s, 1132 s, 1094 s, 1024 s, 928 m, 844 s, 829 s, 803 w, 787 w, 722 vw, 645 vw, 585 w, 558 w, 540 w, 505 w, 406 w. The electronic spectrum is nearly identical to that of **2-PF$_6$**.[6] μ_{eff} (298 K): 1.68 μ_B.

Electrochemistry of the Precursor $Pd_2(DAniF)_4$. Four oxidation processes at 1.274, 1.124, 0.956, and 0.704 V vs Ag/AgCl (Figure 11).

X-ray Crystallography. A single crystal of **1-PF$_6$** was mounted and centered on the goniometer of a Bruker SMART 1000 CCD area detector diffractometer and cooled to −60 °C. Geometric and intensity data were collected using SMART software.[56] The data were processed using SAINT software,[57] and corrections for absorption were applied using the program SADABS.[58]

The structure was solved using the Patterson method, available in the SHELX-97 software package.[59] The cation was found on a special position of space group *P*4/*n* with the Pd−Pd bond lying along the C_4 axis. One of the two independent anisyl groups on the DAniF ligand was disordered in three orientations. The PF_6 anion was also rotationally disordered. All non-hydrogen atoms were refined with anisotropic displacement parameters, and hydrogen atoms were placed in calculated positions. Crystal data are shown in Table 1. Selected bond distances and angles for **1-PF$_6$** are listed in Table 2.

Density Functional Calculations. Calculations at the DFT[60] level were performed with the hybrid Becke 3-parameter exchange functional[61] and the Lee−Yang−Parr nonlocal correlation functional[62]

(55) (a) Cage, B.; Hassan, A. K.; Pardi, L.; Krzystek, J.; Brunel, L. C.; Dalal, N. S. *J. Magn. Reson.* **1997**, *124*, 495. (b) Hassan, A. K.; Pardi, L.; Krzystek, J.; Sienkiewicz, A.; Goy, P.; Rohrer, M.; Brunel, L. C. *J. Magn. Reson.* **2000**, *142*, 300.
(56) *SMART*, version 5.618; Software for the CCD Detector System; Bruker Analytical X-ray Systems: Madison, WI, 1998.
(57) *SAINTPLUS*, version 6.45A; Software for the CCD Detector System; Bruker Analytical X-ray Systems: Madison, WI, 1998.
(58) SADABS program for absorption correction using SMART CCD data based on the method of Blessing: Blessing, R. H. *Acta Crystallogr., Sect. A* **1995**, *51*, 33.
(59) Sheldrick, G. M. *SHELXTL97*; University of Göttingen: Göttingen, Germany, 1997.

Table 2. Selected Bond Distances (Å) and Angles (deg) for **1-PF$_6$**

Pd−Pd	2.597(1)
Pd−N	2.043[6]
Pd···F	4.782
Pd−Pd−N	86.6[2]
N−Pd−N_{trans}	173.3[3]
N−Pd−N_{cis}	89.80[2]
N−Pd−Pd−N torsion angle	1.4

(B3LYP) implemented in the Gaussian 98 (revision A.9) program suite.[63] The model used was $Pd_2(HNCHNH)_4$, in which the aryl groups of the formamidinate ligands were replaced by hydrogen atoms. Geometry optimizations were performed on both neutral and singly oxidized models without any symmetry constraints. Double- and triple-ζ basis sets were used for two separate $Pd_2(HNCHNH)_4$ calculations. The singly oxidized model was calculated using the double-ζ basis set. The double-ζ calculations consisted of the correlation consistent polarized (cc-pVDZ)[64] valence basis set used for nonmetal atoms (carbon, nitrogen, and hydrogen), and an effective core potential (ECP) representing the 1s2s2p3s3p3d core was used for the palladium atoms along with the associated double-ζ basis set (LANL2DZ).[65] The triple-ζ calculations utilized the correlation consistent polarized (cc-pVTZ)[66] basis set for nonmetal atoms and an ECP representing the 1s2s2p3s3p3d core along with the Stuttgart triple-ζ basis set.[67] The self-consistent field cycle criterion for convergence on all calculations was increased from the default value to 10^{-8}. All calculations were run on an Origin 3800 64-processor SGI computer located at the Texas A&M Supercomputing Facility.

Acknowledgment. At TAMU, we thank the Robert A. Welch Foundation and Texas A&M University for financial support and the Laboratory for Molecular Simulation at TAMU for software. J.F.B. thanks the National Science Foundation for a predoctoral fellowship and the Alexander von Humbolt Foundation for a postdoctoral fellowship. We are also grateful to Mr. Brian K. Roberts for assistance with EPR spectroscopy and to Dr. Ronald C. Clark for help with sample preparation for some of the EPR studies. The work at FSU was supported by NSF DMR-0506946 and the National High Magnetic Field Laboratory (NHMFL); NHMFL is operated under the NSF Cooperative Agreement DMR-0084173 and the State of Florida.

Supporting Information Available: X-ray crystallographic data for **1-PF$_6$** in CIF format. D-band EPR spectrum of **1-PF$_6$** at 200 K (Figure S1), second derivative EPR spectrum of **1-PF$_6$** in the presence of BuCN (Figure S2), D-band EPR spectra of $[Pd_2(DTolF)_4]PF_6$ from 100 K down to 5 K (Figure S3), and complete citation for ref 63. This material is available free of charge via the Internet at http://pubs.acs.org.

JA067328Y

(60) (a) Hohenberg, P.; Kohn, W. *Phys. Rev.* **1964**, *136*, B864. (b) Parr, R. G.; Yang, W. *Density-Functional Theory of Atoms and Molecules*; Oxford University Press: New York, 1989.
(61) (a) Becke, A. D. *Phys. Rev. A* **1988**, *38*, 3098. (b) Becke, A. D. *J. Chem. Phys.* **1993**, *98*, 1372. (c) Becke, A. D. *J. Chem. Phys.* **1993**, *98*, 5648.
(62) Lee, C. T.; Yang, W. T.; Parr, R. G. *Phys. Rev. B* **1998**, *37*, 785.
(63) Frisch, M. J.; et al. *Gaussian 98*, revision A.9; Gaussian, Inc.: Pittsburgh, PA, 1998.
(64) Dunning, T. H., Jr. *J. Chem. Phys.* **1989**, *90*, 1007.
(65) (a) Wadt, W. R.; Hay, P. J. *J. Chem. Phys.* **1985**, *82*, 284. (b) Wadt, W. R.; Hay, P. J. *J. Chem. Phys.* **1985**, *82*, 299.
(66) Dunning, T. H., Jr. *J. Chem. Phys.* **1989**, *90*, 1007.
(67) Andrae, D.; Haussermann, U.; Dolg, M.; Stoll, H.; Preuss, H. *Theor. Chim. Acta* **1990**, *77*, 123.